

Hydroxyapatite as Green Catalyst for Environmental Cleaning

Yunzi Xin*, Takashi Shirai*,**

*Advanced Ceramics Research Center, Nagoya Institute of Technology
Gokiso-cho, Showa-ku, Nagoya, Aichi 466-8555, Japan

**Department of Life Science and Applied Chemistry,
Graduate School of Engineering, Nagoya Institute of Technology
Gokiso-cho, Showa-ku, Nagoya, Aichi 466-8555, Japan

Hydroxyapatite, one of the most well-known calcium phosphate compounds, has been extensively applied as a bioceramic for artificial bone tissue crafting, ion-exchange fillers for heavy metal ions, and adsorbents of proteins owing to its unique chemical and physical properties. The application of hydroxyapatite as a green catalyst for the oxidative decomposition of volatile organic compounds (VOCs) opens a new avenue for the design and development of functional ceramic materials. This review summarizes the catalytic decomposition of VOCs on hydroxyapatites under both thermal- and photo-excited conditions, followed by a detailed summary of the correlated chemical structure and surface characteristics, as well as elucidation of the catalytic mechanism.

Keywords: Catalyst, hydroxyapatite, oxidative decomposition, volatile organic compound

The emission of VOCs has become one of the most serious global environmental issues owing to rapid urbanization and industrialization. VOCs emitted from various sources, such as automobiles, chemical manufacturing, and printing, become the most prevalent pollutants in air and water and precursors for photochemical smog and secondary aerosols. Owing to the toxic and carcinogenic nature of VOCs, they also pose short- and long-term harmful impacts on human beings. ^[1-3] Thermal-induced catalytic decomposition of VOCs on porous ceramic-carried noble metal nanoparticles has attracted worldwide attention because this process can oxidize VOCs into CO₂ and H₂O under relatively low temperatures. ^[4-6] However, its high cost, heavy loading amount, and stringent requirement for good dispersibility limit its application. Recently, noble metal-free catalysts, such as metal-doped ceramic complexes (Mn-SBA15, CuCe_xZr_{1-x}O_y/ZSM-5), metal oxides (CoO_x-CeO₂, MnO_x-CeO₂), and perovskites (LaFeO₃, LaNiO₃, LaFe_{1-y}Ni_yO₃) have emerged as efficient catalysts for the oxidative decomposition of VOCs. ^[7-11] Nevertheless, the complex synthetic route and difficulties in precisely controlling the chemical compositions are the main drawbacks of these catalysts. Therefore, the development of alternative noble metal-free catalysts is urgently required to meet sustainable development goals.

Hydroxyapatite (stoichiometric formula:

Ca₁₀(PO₄)₆(OH)₂), a well-known calcium phosphate compound, has been extensively applied in artificial bone tissue crafting, ion-exchange fillers for heavy metal ions, and adsorbents of proteins owing to its unique chemical and physical properties. Both stoichiometric and non-stoichiometric hydroxyapatites with altered Ca/P ratios, controlled crystal morphology, and different particle sizes can be easily synthesized via various strategies, such as liquid-phase precipitation, hydrothermal approach, microwave-assisted method, and high-temperature hydrolysis. ^[12] In the 1990s, Nishikawa et al. started to study the thermal/photocatalytic activities of hydroxyapatites in the oxidative decomposition of VOCs. ^[13] Investigations of the thermal-/photo-excited radical generation phenomenon on hydroxyapatites have progressed in the next several decades. ^[14-17] However, further practical applications for VOC elimination have rarely persisted because of the lack of knowledge and deep understanding of the catalytic mechanism of the hydroxyapatite surface. In 2020, our group unprecedentedly reported the thermal-catalytic mechanism and succeeded in achieving complete decomposition of VOCs on hydroxyapatites, which unlocks a new prospect for the development of noble metal-free catalysts for VOC purification and environmental cleaning owing to their facile preparation, cost-efficiency, and non-toxicity. ^[18] Furthermore, we

reported a novel and facile mechanochemical activation technique of hydroxyapatite, for perusing the deep oxidation of byproducts with 100% CO₂/CO selectivity.^[19] In addition, an active porous hydroxyapatite filter was also successfully developed by utilizing the ceramic shaping process of gel casting, and the results provide direct evidence for the practical application of hydroxyapatite catalysts in manufacturing.^[20]

This review summarizes the catalytic decomposition of VOCs on hydroxyapatites for both thermal- and photo-excited conditions and reveals the corresponding chemical structure and surface characteristic study to elucidate the catalytic mechanism. We believe that the contents of this review can provide important insights for not only the fields of catalytic science and technology but also for the design and development of functional ceramic materials.

1. Thermocatalytic decomposition of VOCs on hydroxyapatites

In 1991, Nishikawa et al. reported the catalytic oxidative decomposition of trichloroethylene (TCE) on calcium-deficient hydroxyapatite (DAP).^[13] The DAP, with a Ca/P molar ratio of 1.54, was synthesized via the liquid-phase precipitation approach with diammonium hydrogen phosphate and calcium nitride as precursors. As shown in **Figure 1a**, catalytic decomposition of TCE was observed on the synthesized DAP in the temperature range of 100–500 °C, while concentration of TCE remained constant when no catalyst was loaded (blank case). The maximum composition efficiency of TCE on DAP was 95% at 500 °C. They also studied the gas species produced at 430 °C and observed the formation of 1,1-dichloroethylene with a trace amount of TCE using gas chromatography (GC) equipped with a flame ionization detector as well as CO₂/CO using GC equipped with a thermal conductivity detector. Regarding the small amount of HCl in the final product, the authors suggested that the generated Cl⁻ might substitute OH⁻ in the DAP structure. However, the detailed reaction mechanism is not clarified in this study. Nishikawa et al. also reported the oxidative decomposition of chlorobenzene on another calcium-deficient hydroxyapatite with a Ca/P molar ratio of 1.58, synthesized using different precursors of calcium oxide and phosphoric acids.^[21] A decomposition efficiency of 43% at 450 °C and the main products of CO₂/CO were obtained for the catalytic decomposition of chlorobenzene. Similar to TCE, the authors also presumed that Cl⁻ was

probably substituted with OH⁻ due to the fact that an enhanced amount of Cl⁻ was detected in the hydroxyapatite sample after the catalytic reaction, which led to a gradual reduction of conversion efficiency upon long-term utilization, as shown in **Figure 1b**. In addition, the authors compared the catalytic activities of DAPs prepared via two different methods: liquid-phase precipitation (DAP-B) and hydrolysis of *α*-tricalcium phosphate (*α*-TCP, DAP-A). Interestingly, *α*-TCP exhibits inactivity toward the catalytic decomposition of chlorobenzene, as summarized in **Figure 1c**. Based on the results of FT-IR (**Figure 1d**), DAP-A exhibits lower crystallinity as the split bands of PO₄ and OH liberations at 630 and 610 cm⁻¹, respectively, were also clearly observed in DAP-A. These results are consistent with the powder X-ray diffraction (PXRD) pattern, which shows that wider peak of (300) in DAP-A (**Figure 1e**). The authors also demonstrated that the activity of calcium-deficient hydroxyapatite can be attributed to its

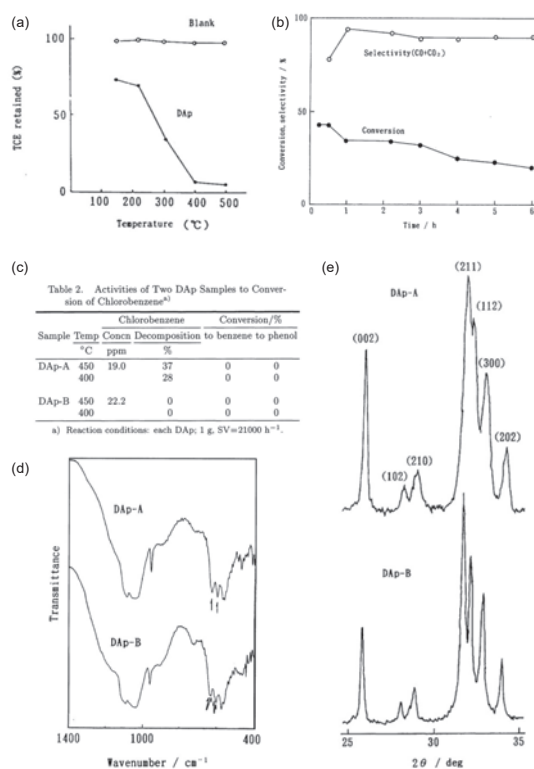


Figure 1. (a) Catalytic decomposition of TCE on DAP, compared with blank (Reprinted from 日本化学誌1991, 11, 1562. Copyright © 1991 The Chemical Society of Japan.). (b) Chlorobenzene conversion and CO₂/CO selectivity using DAP. (c) Comparison of catalytic activities between DAP-B (synthesized via liquid-phase precipitation) and DAP-A (synthesized through hydrolysis of *α*-TCP) by (d) Fourier-transform infrared (FT/IR) and (e) PXRD characterizations. (Reprinted from Bull. Chem. Soc. Jpn., 1994, 67, 2454. Copyright: © 1994 The Chemical Society of Japan.).

much-disordered crystal structure compared with α -TCP.

We previously reported the oxidative decomposition of toluene, ethyl acetate, and isopropanol on thermally excited hydroxyapatites at 400–500 °C.^[22] We used granule-type commercial hydroxyapatites in the size range of 1–2 mm. By systematically comparing with Ca-deficient hydroxyapatite, we found that the stoichiometric hydroxyapatite has the potential to convert VOCs into CO₂/CO owing to the intensified radical generation on the surface, as shown in **Figure 2**. Our group also reported the catalytic decomposition of ethyl acetate on hydroxyapatites with crystal structures oriented along the *a*- or *c*-axis.^[23] In this study, needle-like (HAp-N) and plate-like (HAp-P) hydroxyapatites (**Figure 3a**) were synthesized via air–liquid interface precipitation. The PXRD patterns (**Figure 3e**) demonstrate that HAp-N exhibits a preferred crystal growth of *a*-plane (obvious (300) plane) along *c*-axis, whereas HAp-P exhibits a harvested *c*-plane oriented to *a*(*b*)-axis with only the (002) peak appear. The decomposition rates for HAp-P and HAp-N were evaluated to be 97.8% and 48.4%, respectively. It was demonstrated that HAp-P with a large number of surface OH groups on the

c-plane promotes both the adsorption of ethyl acetate and the generation of active radicals under thermal treatment, resulting in enhanced catalytic activity.

Recently, we reported the oxidative decomposition of VOCs such as ethyl acetate, 2-propanol, and acetone at 400 °C using hydroxyapatites with Ca/P molar ratios of 1.70, 1.67, 1.57, and 1.37. As shown in **Figures 4a,c,e**, the chemical composition of hydroxyapatite plays an important role in catalytic activity. Hydroxyapatite with a Ca/P ratio of 1.67 exhibited superior catalytic activity, and the hydroxyapatite resulted in the complete decomposition of ethyl acetate and isopropanol.^[18] The chemical structures of the gaseous products generated through the catalytic reaction of VOCs were systemically identified for the first time. As shown in **Figures 4b,d,f**, the gaseous products of decomposed ethyl acetate and isopropanol were obtained as ethylene/acetaldehyde/ethanol and propylene/acetone, respectively, whereas no organic compounds were observed for acetone. Based on these results and a detailed investigation on the chemical and physical properties of hydroxyapatites with different Ca/P ratios, the catalysis mechanism was unprecedentedly established in this work, which opens a new prospect for hydroxyapatite as a noble metal-free catalyst for environmental cleaning. Further details are discussed in Section 3. Furthermore, the influence of Ca and P precursors, utilized in the preparation of hydroxyapatite (via liquid-phase precipitation), on the catalytic oxidative decomposition

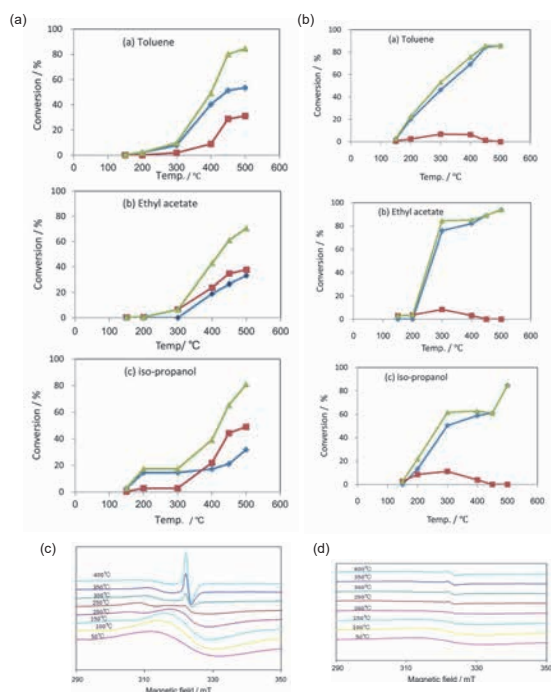


Figure 2. Conversion of toluene, ethyl acetate, and isopropanol on the (a) stoichiometric and (b) Ca-deficient hydroxyapatites. Electron spin resonance (ESR) spectra of the (c) stoichiometric and (d) Ca-deficient hydroxyapatites at different temperatures. (Reprinted from Appl. Surf. Sci. 2012, 258, 5370. Copyright © 2012 Elsevier B. V. All rights reserved.).

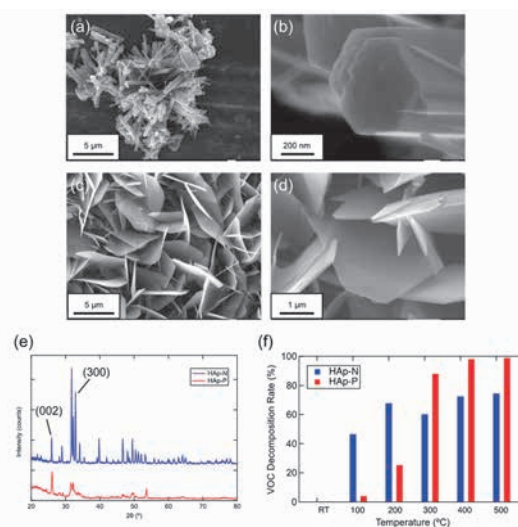


Figure 3. SEM images of (a,b) HAp-N and (c,d) HAp-P. (e) PXRD patterns and (f) VOC decomposition rates of HAp-N and HAp-P. (Reprinted from Journal of the Ceramic Society of Japan 2019, 127, 263. Copyright © 2019 The Ceramic Society of Japan.).

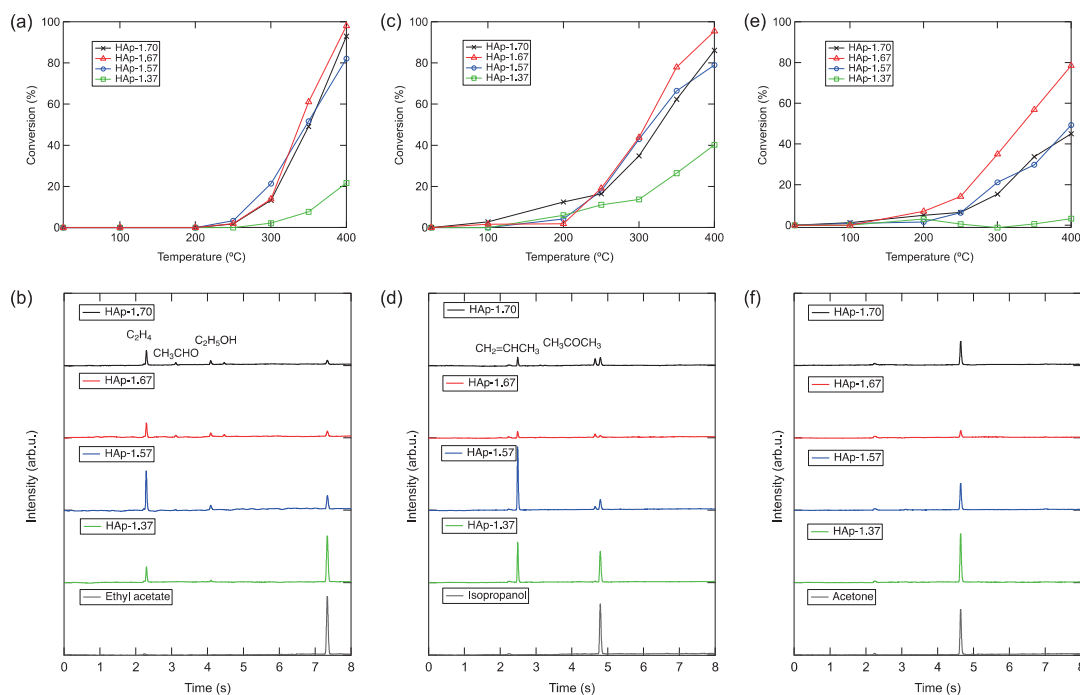


Figure 4. Temperature-dependent conversion efficiencies and GC spectra of gaseous products for various VOCs: (a,b) ethyl acetate (c,d) isopropanol, and (e,f) acetone. (Reprinted from *Catalysis Science & Technology* 2020, 10, 5453. Copyright © The Royal Society of Chemistry 2020.).

of ethyl acetate was also reported by our group.^[24] As shown in **Figure 5a**, four types of hydroxyapatite (HAP-1/2/3/4) with different particle sizes and morphologies were synthesized. It is worth noting that the Ca/P molar ratios for these hydroxyapatites were similar (1.67). It was found that a more efficient CO_2/CO conversion of 80%–100% can be achieved at 400–500 °C by using hydroxyapatites synthesized from the chemical reaction between calcium hydroxide and phosphoric acid (HAP-1 and HAP-2 in **Figures 5b** and **5c**, respectively). In contrast, the catalytic activity of hydroxyapatite was inhibited by the increased acidity induced by the substitution of CO_3^{2-} when calcium carbonate was used as the precursor (HAP-3 and HAP-4 in **Figures 5d** and **5e**, respectively).

In a recent study, we observed 100% CO_2/CO conversion from ethyl acetate on surface-activated stoichiometric hydroxyapatite using a facile mechanochemical treatment.^[19] Hydroxyapatites treated by high-energy planetary ball-milling-induced mechanochemical processes show better catalytic activity than raw powder, indicating that the size of the ball utilized in ball milling plays a major role (**Figures 6a–d**). The predominant defect/oxygen vacancy generation at the PO_4^{3-} site and enhanced basic site population achieved by the selective activation of the c-plane through the planetary ball-milling process are

attributed to the highly efficient catalytic activity with excellent cyclic ability, as shown in **Figure 6e**.

Using a ceramic shaping technique, porous

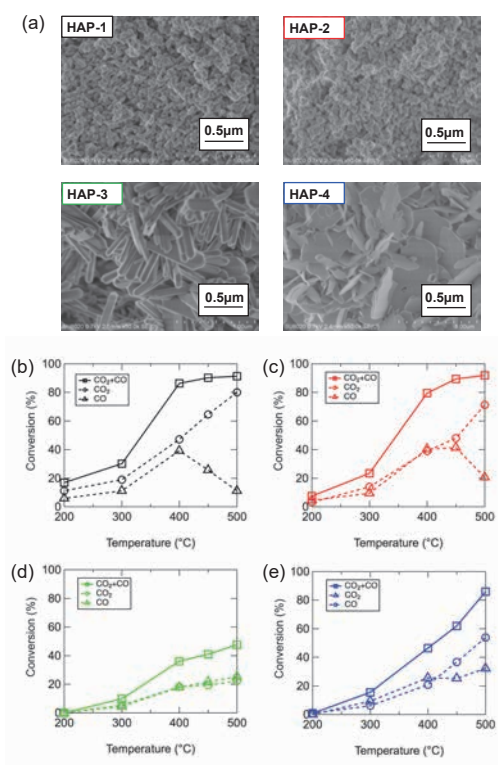


Figure 5. (a) SEM images and (b–e) conversion efficiencies of different hydroxyapatites. (Reprinted from *Journal of the Ceramic Society of Japan* 2021, 129, 601. Copyright © 2021 The Ceramic Society of Japan.).

hydroxyapatite ceramic filters with altered pore structures (**Figure 7a**) were also successfully fabricated via a facile gel-casting process.^[20] The porous hydroxyapatite filters

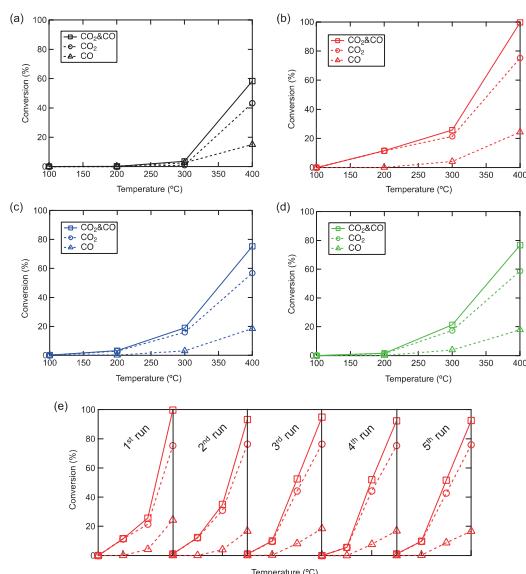


Figure 6. CO₂/CO conversion of ethyl acetate at different temperatures over (a) raw and mechanochemically activated hydroxyapatites using (b) 3 mm, (c) 10 mm, and (d) 15 mm milling balls. (e) Cyclic test results of hydroxyapatite activated using 3 mm milling ball. (Reprinted from Scientific Reports 2021, 11, 7512. Copyright © The Author(s) 2021.).

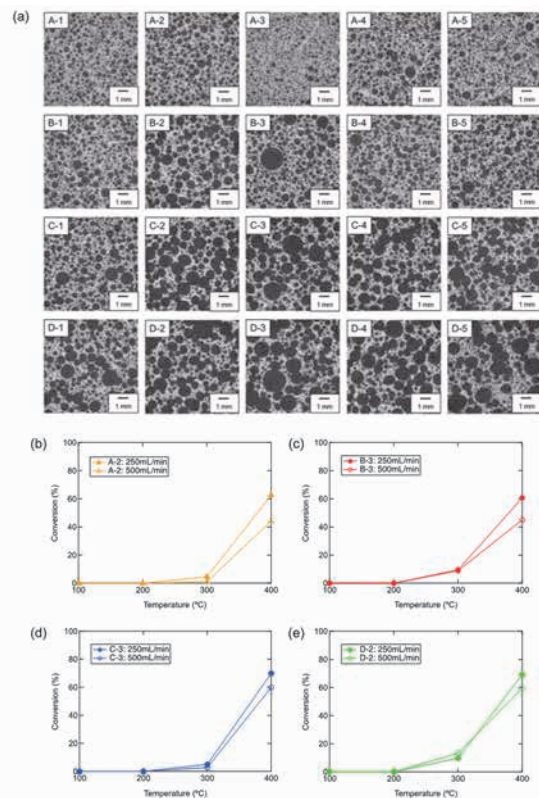


Figure 7. (a) Pore structure of fabricated hydroxyapatite filters observed by X-CT. (b–e) Catalytic decomposition of ethyl acetate using the selected filters in (a). (Reprinted from Scientific Reports 2021, 11, 7512. Copyright © The Author(s) 2021.).

with controlled pore structures exhibited comparable catalytic activity with that of powder in the thermal-oxidative decomposition of ethyl acetate (see details in **Figures 7b–e**). The correlation between the gas permeability of the established pore structure and the catalytic performance of the filter was studied in advance. Without a load of noble metal nanoparticles, the catalytic activity achieved using the hydroxyapatite filter by itself opens a new path for future VOC purification techniques.

2. Photocatalytic decomposition of VOCs using hydroxyapatites

The photocatalytic decomposition of methyl mercaptan (MM) on stoichiometric hydroxyapatite under UV irradiation was reported by Nishikawa et al.^[25] Hydroxyapatite was synthesized by the precipitation of diammonium hydrogen phosphate and calcium nitride precursors. The authors compared the catalytic activities of hydroxyapatites heated at 200 °C (HAp200) and 1150 °C (HAp1150) and found that only HAp200 exhibited catalytic activity towards the decomposition of MM when irradiated with UV light of 254 nm wavelength (**Figure 8**). The authors presumed that the catalytic activity of HAp200 could be attributed to the

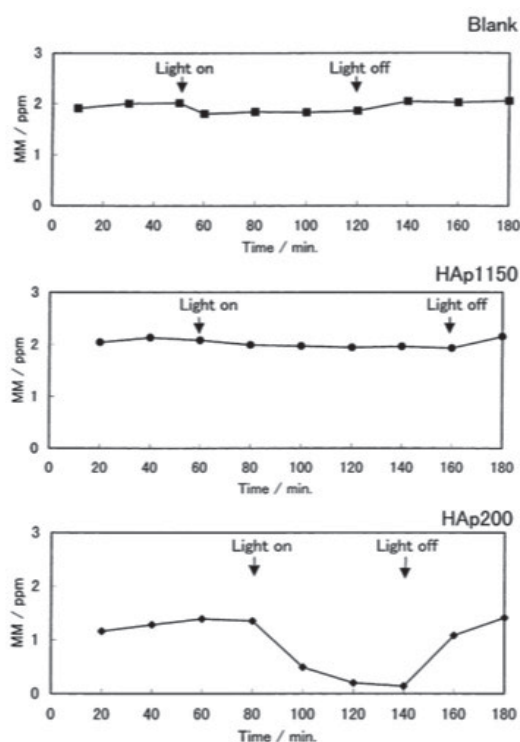


Figure 8. Comparison of the catalytic decompositions of MM using two types of hydroxyapatite under UV light irradiation. (Reprinted from Journal of Molecular Catalysis A: Chemical 2002, 179, 193. Copyright © 2002 Elsevier Science B. V.).

generation of $O_2^{\cdot-}$ radical generated on the surface. The inhibitory activity of HAp1150 was not investigated in their study.

Nishikawa also reported satisfactory photocatalytic decomposition of dimethyl sulfide (DMS) using commercial Ca-rich hydroxyapatite. [26] In comparison with stoichiometric hydroxyapatite (74%–78%) and α -TCP (45%), Ca-rich hydroxyapatite shows a superior photocatalytic activity towards the decomposition of DMS and conversion efficiency of up to 98%–100% (Figure 9). It was assumed that the excellent catalytic performance of Ca-rich hydroxyapatite might be attributed to its high crystallinity towards the a-axis. Although the products of the photocatalytic decomposition of DMS were identified as $SO_2/CO_2/H_2O$, the detailed catalytic mechanism has not been clarified.

3. Structural study of hydroxyapatite and elucidation of the catalytic mechanism

For a better understanding of the hydroxyapatite catalytic mechanism, much effort has been devoted to chemical structure studies. Nishikawa systematically investigated the change in the chemical structure of

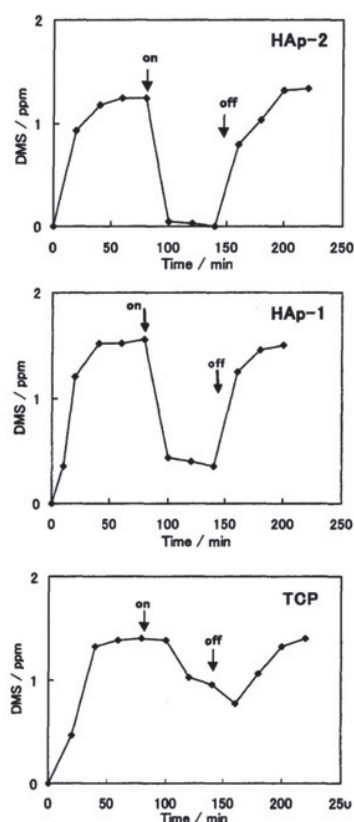


Figure 9. Comparison of the catalytic decompositions of DMS using three types of hydroxyapatite under UV light irradiation. (Reprinted from Journal of Molecular Catalysis A: Chemical 2004, 207, 149. Copyright © 2004 Elsevier Science B. V.).

hydroxyapatite under thermal treatment at different temperatures of 100, 550, 900, and 1150 °C. [15] Based on the sharpness of the PXRD peak observed in the hydroxyapatite samples that were thermally treated at higher temperatures (Figure 10a), it can be concluded that the crystallinity was enhanced. Furthermore, the FT/IR spectra (Figure 10b) revealed that structural water in the apatitic structure was removed at 900–1150 °C. The author mentioned the coloring phenomenon in thermally treated samples. As shown in the absorption spectra (Figure 10c), the order of absorption intensity was 1150 > 550 > 900 > 100 °C, and the results show good agreement with color-changing observations. The significantly increased UV absorption under 400 nm, observed in the sample heated at 1150 °C, suggests a surface structure change in hydroxyapatite. A similar result can be observed in the photoluminescence spectra shown in Figure 10d. The hydroxyapatite samples thermally treated at 900, 550, and 100 °C exhibited fluorescence centers at 320, 400, and 443 nm, respectively, whereas the peak intensity at 320 nm decreased for the sample heated at 1150 °C. The author assumed that this phenomenon might be attributed to the radical formation and investigated the electron state of hydroxyapatite by ESR analysis at -196 °C. The ESR spectra shown in Figure 10e demonstrate that three types of radicals appeared in the hydroxyapatite samples heated at 900 °C ($g = 2.0089/2.0073/2.0006$) and 1150 °C ($g = 2.0185/2.0049/1.9864$). Such radicals were assigned as $O_2^{\cdot-}$ species generated by the reaction between the adsorbed O_2 and electrons. According to the FT/IR analysis, the difference in the g -values of the samples heated at 900 and 1150 °C was assumed to be correlated to the different behaviors of structural water removal.

Radical generation on hydroxyapatite under UV irradiation was previously studied by Kanai et al. [14] and Nishikawa [16]. According to Kanai et al., ESR signals at $g = 2.0599$ and 2.0023 were observed for hydroxyapatite irradiated by an ultrahigh mercury lamp at 77 K (Figure 11a). Such radicals were assigned as $O^{\cdot-}$ species, which were unstable at room temperature. After treatment with oxygen, a further reaction occurred with the $O^{\cdot-}$ species to produce O^{3-} , leading to new ESR signals appearing at $g = 2.002$, 2.011 , and 2.017 . In contrast, hydroxyapatite irradiated at room temperature generated another new type of O^{3-} species with ESR peaks at $g = 2.006$, 2.009 , and 2.0014 (Figure 11b). It has also been demonstrated that this type of O^{3-} species decays faster than that generated at a low temperature of 77 K. The fast decay

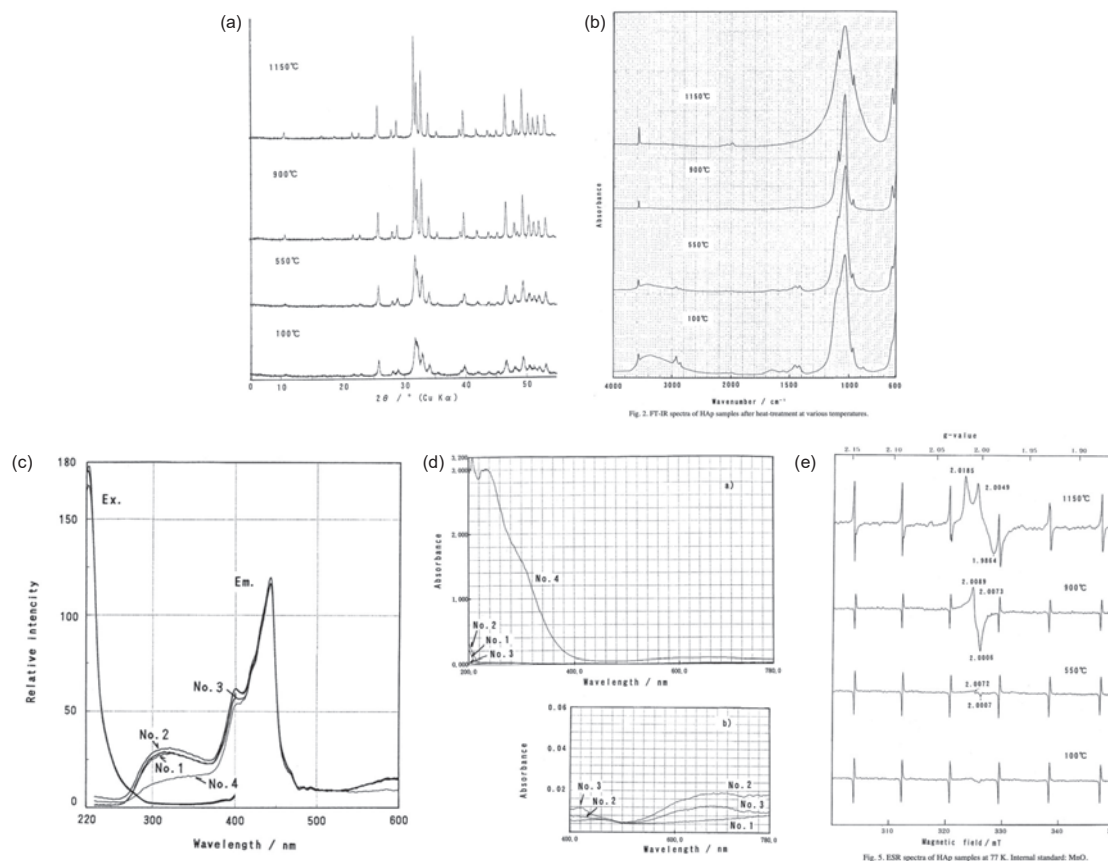


Figure 10. (a) XRD patterns, (b) FT-IR spectra, (c) UV-vis spectra, and (d) photoluminescence spectra of hydroxyapatites pre-heated at different temperatures. (No. 1, 2, 3, and 4 represent samples pre-heated at 100, 550, 900, and 1150 °C, respectively.) (Reprinted from Journal of Molecular Catalysis A: Chemical 2004, 207, 149. Copyright © 2004 Elsevier Science B. V.).

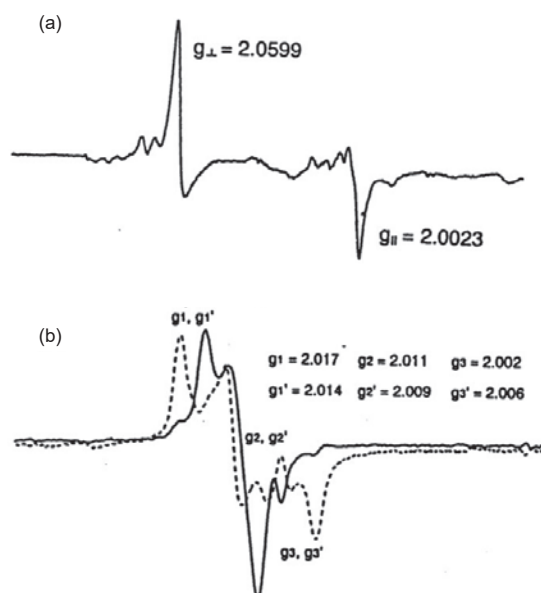


Figure 11. ESR spectra of (a) hydroxyapatite irradiated by an ultrahigh mercury lamp at 77 K and (b) hydroxyapatite samples after treated with oxygen at room temperature (solid line) and after irradiated at room temperature (dashed line). (Reprinted from Phosphorus research Bulletin 1996, 6, 293. Copyright © 1996 日本無機リン化学会.)

of $O^{\cdot-}$ species generated by UV irradiation was attributed to the location of radical in hydroxyapatite; that is, the radical formed through UV on the surface or near the inlet of the channel could easily escape. Instead of low-temperature-treated hydroxyapatite, Nishikawa investigated the UV irradiation-induced radical on hydroxyapatites that were pre-heated at 200 and 1150 °C. In the presence of 3,4-Dihydro-2,2-dimethyl-2H-pyrrole 1-oxide (DMPO)/water, $\cdot OH$ radicals were detected on the photo-induced excitation of hydroxyapatite that was preheated at 200 °C (**Figure 12a**). As shown in **Figure 12b**, the relative intensity of the generated $\cdot OH$ radical increased as the UV irradiation time was extended. In contrast, $O_2^{\cdot-}$ formation was observed in DMPO/dimethyl sulfoxide (DMSO), and the author also demonstrated that such radicals can also be efficiently generated using hydroxyapatite pre-heated at 200 °C (**Figures 12d,e**). Based on the results (**Figure 12c**), the inactive oxygen radical of the 1150-°C preheated hydroxyapatite was assumed to be constrained by the matrix in the hydroxyapatite crystal.

In addition, Nishikawa characterized the chemical

surface change of hydroxyapatite (pre-heated at 200 °C) by UV irradiation using FT/IR and X-ray photoelectron spectroscopy (XPS).^[17] Based on the FT/IR spectra of the hydroxyapatite sample (**Figure 13**), the peaks at 3570, 1030, and 960 cm^{-1} can be assigned to the apatitic OH, ν_3 of PO_4^{3-} , and ν_1 of PO_4^{3-} , respectively. The peak

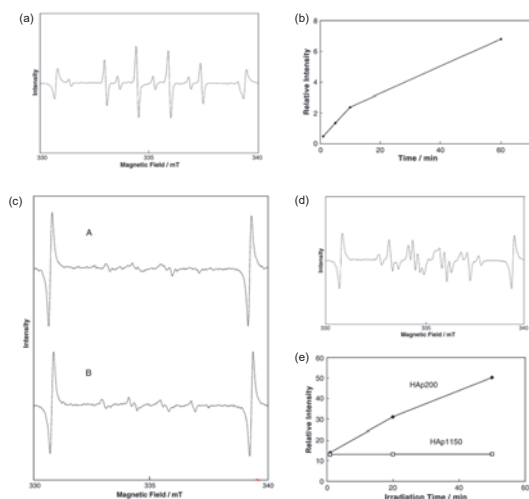


Figure 12. (a) ESR spectra of hydroxyapatite pre-heated at 200 °C after UV irradiation for 1 min (DMPO/H₂O). (b) Plot of the relative intensity of ·OH signal vs. irradiation time. (c) ESR spectra of hydroxyapatite pre-heated at 1150 °C after UV irradiation for 1 min (DMPO/DMSO). (d) Comparison of the ESR signals between the hydroxyapatite samples pre-heated at 200 and 1150 °C after UV irradiation for 1 min (DMPO/DMSO). (Reprinted from Materials Letters 2003, 58, 14. Copyright © 2003 Elsevier B. V.).

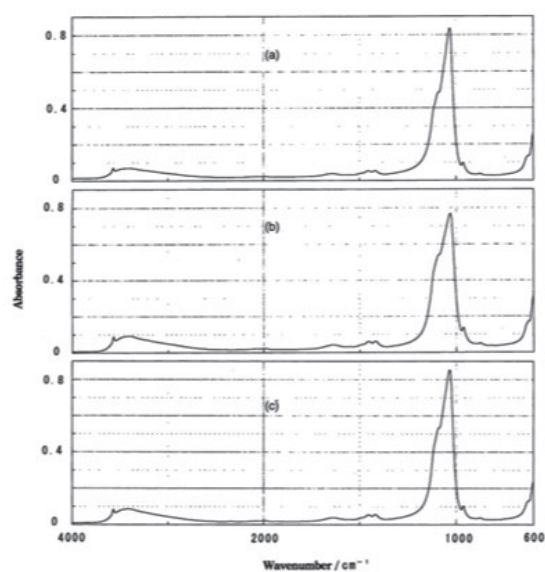


Figure 13. FT/IR spectra of hydroxyapatite pre-heated at 200 °C (a) before UV irradiation, (b) after UV irradiation, and (c) after further standing for 1 h. (Reprinted from Journal of Molecular Catalysis A: Chemical 2003, 206, 331. Copyright © 2003 Elsevier B. V.).

intensity of ν_3 of PO_4^{3-} was obviously decreased after UV irradiation; thus, the structural change of the surface PO_4^{3-} probably occurred on the photo-induced excitation of hydroxyapatite. Accordingly, the binding energy shifts and recoveries of Ca_{2p} , P_{2p} , and O_{1s} to lower energy levels (0.05–0.10 eV) were also confirmed by XPS analysis (**Figure 14**), which demonstrates that the UV-irradiated hydroxyapatite is negatively charged due to the radicals generated on the surface. Additionally, Nishikawa conducted an ESR analysis on hydroxyapatite preheated at 1150 °C, and the results are displayed in **Figure 15**. Although stable O_2^- ($g = 2.0180/2.0053/1.9878$) and O^- ($g = 2.0693/2.0651$) radicals were detected for the 1150-°C pre-heated hydroxyapatite before and after UV irradiation, respectively, these species were described as inactive states because hydroxyapatite pre-heated at 1150 °C showed no activity in the photocatalytic decomposition of MM. In contrast, for the 200 °C pre-heated hydroxyapatite, the signal at $g = 2.003$ appears by subtracting the ESR spectra before and after UV irradiation, as shown in **Figure 16**. This signal was attributed to the trapped electron in the hydroxyapatite vacancy, probably induced by the surface PO_4^{3-} site as

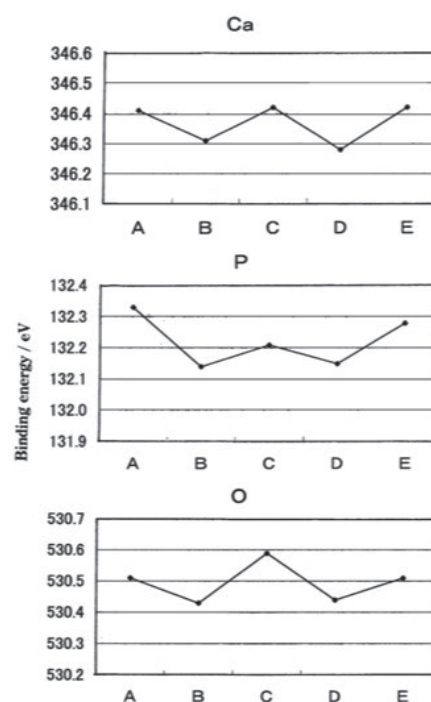


Figure 14. Changes of binding energy summarized from the XPS measurement of hydroxyapatite pre-heated at 200 °C. (A, before UV irradiation; B, after UV irradiation; C, after standing for 1 h after UV irradiation; D, UV re-irradiation; and E, after standing for 1 h after UV re-irradiation.) (Reprinted from Journal of Molecular Catalysis A: Chemical 2003, 206, 331. Copyright © 2003 Elsevier B. V.).

indicated by the FT/IR results. Thus, the author suggested a different photocatalytic mechanism for hydroxyapatite than proposed by Kanai et al.; that is, the trapped electron in the vacancy of hydroxyapatite led to a further formation of $O_2^{\cdot-}$ via reaction with adsorbed oxygen molecules, which oxidize the VOCs.

Owing to the lack of detailed characterization of products produced through the catalytic reaction of VOC, the catalysis mechanism for hydroxyapatite has rarely been clarified. In 2020, a detailed reaction mechanism was initially derived by our group with the assistance of a systematic investigation of the particle morphology, crystallinity, surface acidic/basic properties, thermally activated radical generation dynamics, surface VOC affinity of hydroxyapatites with

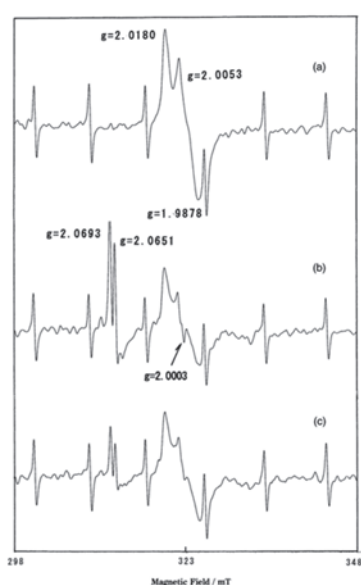


Figure 15. ESR spectra of hydroxyapatite pre-heated at 1150 °C by an ultrahigh mercury lamp at 77 K: (a) before UV irradiation, (b) after UV irradiation, and (c) after standing for 1 h after UV irradiation. (Reprinted from *Journal of Molecular Catalysis A: Chemical* 2003, 206, 331. Copyright © 2003 Elsevier B. V.).

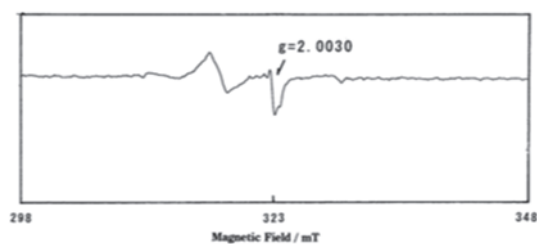


Figure 16. Substrate ESR spectrum of hydroxyapatite pre-heated at 200 °C before and after UV irradiation. (Reprinted from *Journal of Molecular Catalysis A: Chemical* 2003, 206, 331. Copyright © 2003 Elsevier B. V.).

altered Ca/P ratios, and the chemical structure of gaseous products of VOCs such as ethyl acetate, 2-propanol, and acetone during catalytic decomposition.^[18] In addition to the previously mentioned oxygen radical-induced oxidation reaction of VOCs, we emphasize the important role of the surface VOC adsorption properties as well as the unique acidity/basicity of the hydroxyapatite surface in the step-by-step decomposition of VOCs, as summarized in **Figure 17**. As shown in the ESR spectra of hydroxyapatites with altered Ca/P ratios (**Figure 17a**), a signal with a g value of 2.003 corresponding to trapped electron appeared in samples with Ca/P of 1.67 and 1.70, whose value shifted to 2.002 in calcium-deficient cases. The ESR signal intensity was further compared (**Figure 17b**), and the results suggest that radical generation greatly depends on the chemical composition of the hydroxyapatites. Meanwhile, based on the in-situ FT/IR spectra for the VOC adsorption characterization (**Figure 17c**) and the resultant estimation of adsorption amount (**Figure 17d**), it can be concluded that the VOC affinity on the hydroxyapatite surface varied with the Ca/P ratios. In addition, the results of the quantification of surface acidic and basic sites (**Figure 17e**) suggest that stoichiometric hydroxyapatite possesses the highest population of basic sites on the surface, whereas many more acidic sites are present on calcium-rich and calcium-deficient hydroxyapatites because of the large

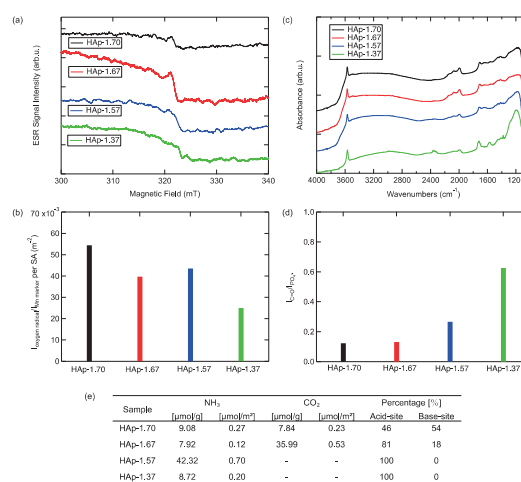
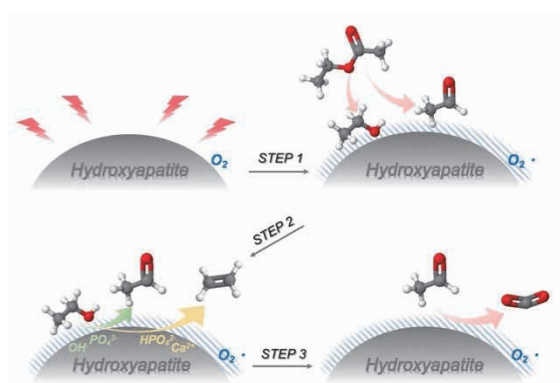


Figure 17. (a) ESR spectra of hydroxyapatites with altered Ca/P molar ratios. (b) Comparison of the ESR signal intensity for different hydroxyapatites. (c) In-situ FT/IR spectra of hydroxyapatites with ethyl acetate flow. (d) Quantification adsorption of ethyl acetate on different hydroxyapatites. (e) Populations of surface acidic and basic sites. (Reprinted from *Catalysis Science & Technology* 2020, 10, 5453. Copyright © The Royal Society of Chemistry 2020.

amounts of Ca^{2+} and HPO_4^{2-} . Based on the GC results (**Figure 4**), we propose the catalytic decomposition mechanism of VOC, for example, ethyl acetate, as follows. First, ethyl acetate decomposes into acetaldehyde and ethanol via reactions with thermally induced oxygen radicals. Second, the generated ethanol transforms into ethylene via dehydration on the acidic sites of Ca^{2+} (as well as HPO_4^{2-}), whereas acetaldehyde can also be produced via the oxidation of ethanol on the basic site surfaces of PO_4^{3-} and OH^- . Finally, the acetaldehyde generated in the first and second steps directly oxidizes into CO_2 and CO via the superactivity of oxygen radicals. The catalytic mechanism is illustrated in **Scheme 1**. The mechanism can also be adapted for the catalytic decomposition of acetate, alcohol, aldehyde, and ketone.

In conclusion, this review summarizes the application of hydroxyapatite as a green catalyst for the thermo/photocatalytic oxidative decomposition of VOCs. Following the investigation of the chemical and physical properties of hydroxyapatites under thermal/photoexcitation with respect to radical generation, surface chemical state, VOC affinity, and surface acidity/basicity, the catalytic mechanism of hydroxyapatites is elucidated. We believe that the contents of this review can provide important information for the future design and development of noble metal-free catalysts for VOC purification and environmental cleaning.



Scheme 1. Derived catalytic reaction mechanism of ethyl acetate on the hydroxyapatite surface. (Reprinted from *Catalysis Science & Technology* 2020, 10, 5453. Copyright © The Royal Society of Chemistry 2020.

Reference

- [1] P. M. Lemieux, C. C. Lutgers and D. A. Santoianni, *Prog. Energy Combust. Sci.*, 2004, **30**, 1-32.
- [2] M. Placet, C. O. Mann, R. O. Gibert and M. J. Niefer, *Atmos. Environ.*, 2000, **34**, 2183-2204.
- [3] Y. Huang, S.S.H. Ho, Y. Lu, R. Niu, L. Xu, J. Cao and S. Lee, *Molecules*, 2016, **21**, 56.
- [4] C. He, J. Cheng, X. Zhang, M. Douthwaite, S. Pattison and Z. Hao, *Chem. Rev.*, 2019, **119**, 4471.
- [5] Y. Guo, M. Wen, G. Li and T. An, *Appl. Catal. B: Environ.*, 2021, **281**, 119447.
- [6] H. Huang, Y. Xu, Q. Feng and D. Y. C. Leung, *Catal. Sci. Technol.*, 2015, **5**, 2649.
- [7] H. Perez, P. Navarro and J. J. Delgado, *Appl. Catal. A: General*, 2011, **400**, 238.
- [8] S. Li, Q. Hao, R. Zhao, D. Liu, H. Duan and B. Dou, *Chem. Eng. J.*, 2016, **285**, 536.
- [9] S. Akran, Z. Wang, L. Chen, Q. Wang, G. Shen, N. Han, Y. Chen and G. Ge, *Catal. Comm.*, 2016, **73**, 123.
- [10] D. Delimaris, T. Ioannides, *Appl. Catal. B: Environ.*, 2008, **84**, 303.
- [11] G. Pecchi, P. Reyes, R. Zamora, L. E. Cadus and J. L. G. Fierro, *J. Solid State Chem.*, 2008, **181**, 905.
- [12] K. Lin, C. Wu and J. Chang, *Acta Bio.* 2014, **10**, 4071.
- [13] H. Harumitsu and H. Monma, *日本化学会誌*, 1991, **11**, 1562.
- [14] H. Kanai, Y. Matsumura and J. B. Moffat, *Phosphorus Research Bulletin*, 1996, **6**, 293.
- [15] H. Harumitsu, *Mater. Lett.* 2001, **50**, 364.
- [16] H. Nishikawa, *Mater. Lett.*, 2003, **58**, 14.
- [17] H. Nishikawa, *J. Molecular Catal. A: Chem.*, 2003, **206**, 331.
- [18] Y. Xin, Y. Ando, S. Nakagawa, H. Harumitsu and T. Shirai, *Catal. Sci. Technol.*, 2020, **10**, 5453.
- [19] Y. Xin and T. Shirai, *Sci. Rep.*, 2021, **11**, 7512.
- [20] Y. Xin, S. Nakagawa, H. Harumitsu and T. Shirai, *Ceram. Int.*, 2021, **47**, 11819.
- [21] H. Harumitsu and H. Monma, *Bull. Chem. Soc. Jpn.*, 1994, **67**, 2454.
- [22] H. Harumitsu, T. Oka, N. Asai, H. Simomichi, T. Shirai and M. Fuji, *Appl. Surf. Sci.*, 2012, **258**, 5370.
- [23] Y. Xin, H. Ikeuchi, J. Hong, H. Harumitsu and T. Shirai, *J. Ceram. Soc. Jpn.*, 2019, **127**, 263.
- [24] S. Nakagawa, Y. Xin, H. Harumitsu, Y. Inomata, R. Oyama, T. Namikawa, M. Yamada and T. Shirai, *J. Ceram. Soc. Jpn.*, 2021, **129**, 601.
- [25] H. Nishikawa and K. Omamiuda, *J. Molecular Catal. A: Chem.*, 2003, **179**, 193.
- [26] H. Nishikawa, *J. Molecular Catal. A: Chem.*, 2004, **207**, 149.